tion of Transition Data," *Air Force Boundary Layer Transition Study Group Meeting*, Rept. BSD-TR-67, Vol. II, Sec. 13, Aug. 1967; AIAA Paper 68-669, Los Angeles, Calif., 1968.

[14] Liepmann, H. W., "Investigation of Boundary-Layer Transition on Concave Walls," ACR 4J28, Feb. 1945, NACA.

[15] Smith, A. M. O. and Clutter, D. W., "Solution of the Incompressible Laminar Boundary-Layer Equations," *AIAA Journal*, Vol. 3, No. 4, April 1963, pp. 639–647.

[16] Jaffe, N. A. and Okamura, T. T., "The Transverse Curvature Effect on the Incompressible Laminar Boundary Layer for Longitudinal Flow Over a Cylinder," *Zeitschrift fur Angewandte Mathematik und Physik*, Vol. 19, Fasc. 4, 1968, pp. 564–574.

[17] Wells, Jr., C. S., "Effects of Freestream Turbulence on Boundary-Layer Transition," *AIAA Journal*, Vol. 5, No. 1, Jan. 1967, p. 172.

[18] Von Doenhoff, A. E., "Investigation of the Boundary Layer About a Symmetrical Airfoil in a Wind Tunnel of Low Turbulence," Rept. L-507, Aug. 1940, NACA.

[19] Wetmore, J. W., Zalovcik, J. A., and Platt, R. C., "A Flight Investigation of the Boundary-Layer Characteristics and Profile Drag of the NACA 35-215 Laminar-Flow Airfoil at High Reynolds Numbers," Rept. L-532, May 1941, NACA.

[20] Braslow, A. L. and Visconte, F., "Investigation of Boundary-Layer Reynolds Number for Transition on a NACA $65_{(215)}$-114 Airfoil in the Langley Two-Dimensional Low-Turbulence Pressure Tunnel," TN 1704, Oct. 1948, NACA.

[21] Boltz, F. W., Kenyon, G. C., and Allen, C. Q., "Measurements of Boundary-Layer Transition at Low Speed on Two Bodies of Revolution in a Low Turbulence Tunnel," RM A56G17, 1956, NACA.

FEBRUARY 1970 AIAA JOURNAL VOL. 8, NO. 2

Hypersonic Similarity Solutions for Airfoils Supporting Exponential Shock Waves

J. D. Cole* and Jerome Aroesty†
The RAND Corporation, Santa Monica, Calif.

The flow behind concave and convex exponential shock waves is investigated from the viewpoint of inviscid, hypersonic small-disturbance theory. The supporting two-dimensional airfoil surfaces (which are in general not exponential) are determined, and the optimum such lifting surface, in terms of maximum $C_L^{3/2}/C_D$ for fixed C_D is shown to be only slightly more concave than a flat plate, and the improvement in performance over a flat plate is small. A limit line is shown to exist in the flowfield behind convex exponential shock waves, so that it is not possible to construct an airfoil that supports an exponential shock wave over its entire length if the nose curvature is too large. It is also indicated that this relatively refined theory must be used for studies of performance and optimization, since the results of Newtonian theory are only qualitatively applicable if γ is not unity.

Nomenclature

c^2 = $(\gamma - 1)/2\gamma$
C_L = $L/(\rho_\infty U^2/2)$, $C_D = D/(\rho_\infty U^2/2)$
D = drag
$F(x)$ = dimensionless body height
L = lift
P = pressure
p = dimensionless pressure [see Eq. (5)]
p^* = $(\gamma + 1)/2p$ [see Eq. (28)]
q = velocity
$S(x)$ = dimensionless shock height
U = freestream velocity
u,v = dimensionless velocity components
v^* = $(\gamma + 1)/2v$ [see Eq. (29)]
X = $x - \xi$ (distance from shock along streamline)
γ = specific heat ratio, C_p/C_V
δ = thickness ratio
θ = dimensionless shock slope
ξ = x location of streamline, where it crosses the shock wave
ρ = density
σ = density ratio [see Eq. (6)]
ψ = stream function

Received February 3, 1969; revision received July 17, 1969. This research is supported by the United States Air Force under Project RAND. Views or conclusions contained in this study should not be interpreted as representing the official opinion or policy of the United States Air Force.

* Consultant to The RAND Corporation.
† Engineer Environmental Sciences Dept., The RAND Corporation. Member AIAA.

I. Introduction

THE applications of hypersonic gas dynamics have in recent years been concerned with various aspects of reentry and missile phenomenology, whereas the development of criteria for the study and optimization of lifting and control surfaces has not been actively pursued. Because of this, there are few theoretical results relevant to the estimation of shock-wave/body interference phenomena and to the prediction of the effects of surface shape on control effectiveness in hypersonic flight. However, one well-known result, the "Newtonian chine strip," obtained using Newtonian gas dynamics, suggests that for a fixed drag penalty, surface concavity can result in an enhanced lift-to-drag ratio.

In the present paper this conjecture is subjected to a systematic investigation, in which the flowfield over a class of two-dimensional lifting surfaces (those which support exponential shock waves) is examined from the viewpoint of inviscid, hypersonic small-disturbance theory, and the effect of varying surface concavity on lift-to-drag ratio is then determined for fixed drag.

For $M_\infty = \infty$ and in the framework of inviscid, hypersonic small-disturbance theory, hypersonic similarity solutions with power law shocks and corresponding power law body shapes are well known.‡ In Ref. 3, it is indicated that a limiting case of similar flowfields with power law shocks is the flow-

‡ See Refs. 1 and 2 for a review of these results.

field formed with an exponential shock wave. If $\gamma \neq 1$, exponential shock waves are not supported by exponential bodies. However, only the case of airfoils concave to the oncoming stream is considered in Ref. 3, and further, the results are not presented in a form that makes it easy to study a family of airfoils with various radii of curvature at the nose.

The same formulation is used here for both families of concave and convex airfoils. In addition, the results are presented in such a way that the family of solutions corresponding to different curvature at the nose can be easily studied.

The present analysis neglects any viscous effects. For the present theory to be valid and the customary ideas of inviscid aerodynamics to be applicable, it is necessary that all boundary layers be thin, and attached to the surface. Whether or not these conditions are met in the presence of the adverse pressure gradients that result from surface concavity in a hypersonic flow has not yet been determined.§

II. Hypersonic Small-Disturbance Theory

Consider a slender airfoil whose profile is given by

$$\bar{y} = \delta F(x),\ 0 \leq x \leq 1,\ F(0) = 0,\ F(1) = 1 \tag{1}$$

and the associated shock wave

$$\bar{y} = \delta S(x) \tag{2}$$

in the uniform hypersonic stream (Fig. 1) corresponding to the limiting case that the hypersonic similarity parameter

$$\mathcal{K} = 1/M_\infty^2\delta^2 \to 0 \tag{3}$$

For the inviscid flow of a perfect gas the hypersonic small-disturbance expansion,[1] based on the idea that the thickness ratio $\delta \to 0$, represents the flow quantities as follows¶:

velocity

$$\mathbf{q}(x,\bar{y})/U = \mathbf{i} + \mathbf{j}\delta v(x,y) + \ldots \tag{4}$$

pressure

$$[\bar{P}(x,\bar{y}) - \bar{P}_\infty]/\rho_\infty U^2 = \delta^2 p(x,y) + \ldots \tag{5}$$

density

$$\rho/\rho_\infty = \sigma(x,y) + \ldots \tag{6}$$

where

$$y = \bar{y}/\delta \tag{7}$$

The corresponding flow equations are those of unsteady flow in a cross plane

continuity

$$\partial\sigma/\partial x + v\partial\sigma/\partial y + \sigma\partial v/\partial y = 0 \tag{8}$$

transverse momentum

$$\partial v/\partial x + v\partial v/\partial y + (1/\sigma)\partial p/\partial y = 0 \tag{9}$$

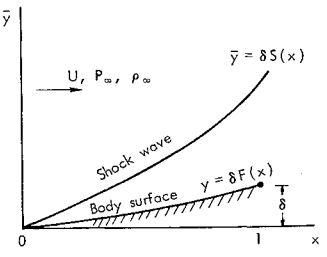

Fig. 1 Coordinate system (hypersonic small-disturbance theory).

§ It is assumed that the surfaces we consider correspond to the lower surface of a two-dimensional wing, whereas the upper surface makes negligible contribution to lift or drag.

¶ Note that the barred quantities are dimensional.

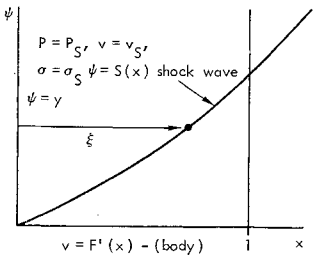

Fig. 2 Domain of boundary value problem (ψ, x plane).

entropy

$$(\partial/\partial x + v\partial/\partial y)p/\sigma^\gamma = 0 \tag{10}$$

The shock jump conditions expressed in terms of shock geometry are

$$p[x,S(x)] = [2/(\gamma+1)]S'^2(x) \tag{11}$$

$$v[x,S(x)] = [2/(\gamma+1)]S'(x) \tag{12}$$

$$\sigma[x,S(x)] = (\gamma+1)/(\gamma-1) \tag{13}$$

The boundary condition of tangent flow at the airfoil surface becomes

$$v[x,F(x)] = F'(x) \tag{14}$$

It is convenient to introduce some auxiliary coordinates, the first of which is the (dimensionless) stream function $\psi(x,y)$ defined by

$$\sigma = \partial\psi/\partial y,\ \sigma v = -\partial\psi/\partial x \tag{15}$$

The independent variables are changed from (x,y) to (x,ψ) by the following differential operations:

$$\partial/\partial x \to \partial/\partial x - \sigma v\partial/\partial\psi$$

$$\partial/\partial y \to \sigma\partial/\partial\psi$$

and the derivative along the streamline (ψ = const) is

$$\partial/\partial x + v\partial/\partial y \to \partial/\partial x$$

Using these transformations, the equations of motion [Eqs. (8–10)] become

$$\partial\sigma/\partial x + \sigma^2\partial v/\partial\psi = 0 \tag{16}$$

$$\partial v/\partial x + \partial p/\partial\psi = 0 \tag{17}$$

$$p/\sigma^\gamma = k(\psi) \tag{18}$$

Here the function $k(\psi)$, the entropy constant on a streamline, can be evaluated parametrically from Eqs. (11) and (13) by using the fact that $\psi = y(\sigma = 1)$ upstream of the shock. On the shock wave

$$\psi[x,S(x)] = \psi_S = S(x) \tag{19}$$

The boundary value problem in the (ψ,x) plane appears in Fig. 2. It is convenient now to replace the coordinate ψ by the coordinate ξ (constant on a streamline) which gives the x location of a streamline where it crosses a shock wave. As a result of this transformation, the domain of the independent variables is fixed, but the shock shape appears in the differential equations. The shock location is given by $x = \xi$, and the shock relations are rewritten

$$p(\xi,\xi) = p_S = [2/(\gamma+1)]\theta^2(\xi) \tag{20}$$

$$v(\xi,\xi) = v_S = [2/(\gamma+1)]\theta(\xi) \tag{21}$$

$$\sigma(\xi,\xi) = \sigma_S = (\gamma+1)/(\gamma-1) \tag{22}$$

where

$$\theta(\xi) = S'(\xi) = \text{shock slope}$$

Since

$$\theta(\xi)\partial/\partial\psi = \partial/\partial\xi$$

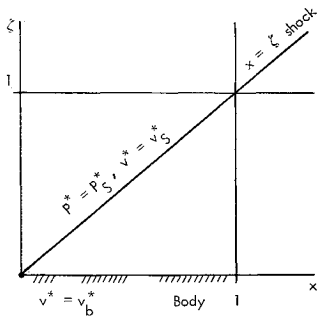

Fig. 3 Domain of boundary value problem (x ξ plane).

the pair of Eqs. (16) and (17) become

$$\theta(\xi)(\partial/\partial x)(1/\sigma) - \partial v/\partial\xi = 0 \tag{23}$$

$$\frac{\partial p}{\partial \xi} + \theta(\xi)\frac{\partial v}{\partial x} = 0 \tag{24}$$

The density can be eliminated from this system by using the entropy integral Eq. (18)

$$\frac{p(x,\xi)}{\sigma^\gamma(x,\xi)} = \frac{[2/(\gamma+1)]\theta^2(\xi)}{[(\gamma+1)/(\gamma-1)]^\gamma} \tag{25}$$

The resulting pair of equations for (p, v) are

$$\frac{1}{\gamma}\left(\frac{\gamma-1}{\gamma+1}\right)\left(\frac{2}{\gamma+1}\right)^{1/\gamma}\frac{\theta(\xi)^{(2/\gamma)+1}}{p^{(1/\gamma)+1}}\frac{\partial p}{\partial x} + \frac{\partial v}{\partial \xi} = 0 \tag{26}$$

$$\partial p/\partial\xi + \theta(\xi)\partial v/\partial x = 0 \tag{27}$$

Finally, it is convenient to scale the variables with the factor $2/(\gamma+1)$. Then

$$p(x,\xi) = 2/(\gamma+1)p^*(x,\xi) \tag{28}$$

$$v(x,\xi) = 2/(\gamma+1)v^*(x,\xi) \tag{29}$$

and we obtain the following forms of the continuity and momentum equations, shock relations, and boundary conditions of tangent flow:

$$c^2\frac{\theta(\xi)^{(2/\gamma)+1}}{p^{*(1/\gamma)+1}}\frac{\partial p^*}{\partial x} + \frac{\partial v^*}{\partial \xi} = 0,\ c^2 = \frac{\gamma-1}{2\gamma} \tag{30}$$

$$\partial p^*/\partial\xi + \theta(\xi)\partial v^*/\partial x = 0 \tag{31}$$

shock conditions:

$$p^*(\xi,\xi) = p^*_s = \theta^2(\xi) \tag{32}$$

$$v^*(\xi,\xi) = v^*_s = \theta(\xi) \tag{33}$$

boundary condition on body surface:

$$v^*(x,0) = v_b^*(x) \tag{34}$$

where

$$v_b^*(x) = \frac{(\gamma+1)}{2}F'(x)$$

The domain of the problem ($x \geq \xi$) is shown in Fig. 3. The special solution corresponding to exponential shock wave shapes for the boundary value problem just formulated is discussed in Sec. III.

III. Similarity Solutions with Exponential Shock Shape

If solutions to Eqs. (30) and (31) are sought by means of separation of variables in the form $f(\xi)g(x-\xi)$, it is seen that solutions can only be found when $f(\xi) \backsim e^{a\xi}$ and correspondingly $\theta(\xi) \backsim e^{a\xi}$. (See Appendix for details.) Thus let

$$p^*(x,\xi) = A^2e^{2a\xi}P(X) \tag{35}$$

$$v^*(x,\xi) = Ae^{a\xi}V(X) \tag{36}$$

where $X = x - \xi$ = distance from shock along a streamline

$$\theta(\xi) = Ae^{a\xi} = S'(\xi) \tag{37}$$

The shock shape is thus

$$S(\xi) = (A/a)(e^{a\xi} - 1) \tag{38}$$

where $a > 0$ yields a concave shock and corresponding concave airfoil, and $a < 0$ corresponds to a convex nose shape. The parameters A, a are not independent but are related by the normalization $F(1) = 1$. Thus a one-parameter family of solutions is obtained.

The shock conditions, Eqs. (32) and (33), are satisfied by

$$P(0) = V(0) = 1,\ X = 0 \text{ on the shock} \tag{39}$$

Under the form of solution assumed previously, the differential equations, Eqs. (30) and (31), become ordinary differential equations

$$(c^2/P^{(1/\gamma)+1})(dP/dX) + aV - (dV/dX) = 0 \tag{40}$$

$$2aP - dP/dX + dV/dX = 0 \tag{41}$$

Elimination between these two equations yields

$$[(c^2/P^{(1/\gamma)+1}) - 1](dP/dX) = -a(V + 2P) \tag{42}$$

$$[(c^2/P^{(1/\gamma)+1}) - 1](dV/dX) = -a[(2c^2/P^{1/\gamma}) + V] \tag{43}$$

Thus the solution can be studied in a (P, V) phase plane with integral curves defined by

$$(dP/dV) = (V + 2P)/(V + 2c^2P^{-(1/\gamma)})$$

$$c^2 = [(\gamma-1)/2\gamma] \tag{44}$$

The corresponding mapping along an integral curve to the physical coordinate X can be found from Eq. (42)

$$adX = [1 - (c^2/P^{(1/\gamma)+1})]dP/(V + 2P) \tag{45}$$

In view of the initial condition, Eq. (39), only the integral curve passing through $P = V = 1$ need be considered and, for all reasonable values of γ, $(P,V) > 0$. A sketch of the integral curve is given in Fig. 4 for a typical γ. The shape of the integral curve in the (P,V) plane depends only on γ. There are no singular points of Eq. (44) in the quadrant $(P,V) > 0$.

Since $c^2 < 1$, the mapping formula, Eq. (45), indicates that X increases as P increases along the path for $a > 0$. This branch of the integral curve corresponds to the concave nose shape. The values of X are found by integrating Eq. (45) along the curve up to the final point (P_T,V_T) where $X = 1$, for a given value a. For other values a, the integration is scaled accordingly. The shape of the body corresponding to this shock shape (given γ,a) is found from the knowledge of $V(X)$, since from Eqs. (36, 34, and 29), it follows that

$$v^*(x,0) = AV(x) = [(\gamma+1)/2]F'(x) \tag{46}$$

The shape is not exponential. The normalization $F(1) = 1$

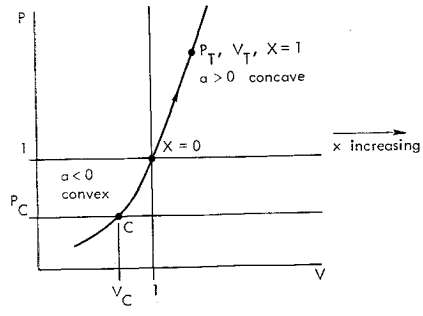

Fig. 4 Integral curves in P, V plane (sketch).

can be used to find A since

$$F(x) = \frac{2}{\gamma + 1} A \int_0^x V(X)\, dX \tag{47}$$

By using Eq. (40), this can be expressed simply as

$$F(x) = \frac{2}{\gamma + 1} \frac{A}{a} \left\{ [V(x) - 1] + \gamma c^2 \left(\frac{1}{P(x)^{1/\gamma}} - 1 \right) \right\} \tag{48a}$$

leading to

$$F(1) = 1 = \frac{2}{\gamma + 1} \frac{A}{a} \left[(V_T - 1) + \gamma c^2 \left(\frac{1}{P_T{}^{1/\gamma}} - 1 \right) \right] \tag{48b}$$

where the subscript T refers to the tail station. The pressure distribution $P(X)$ along the surface is also known.

For the convex bodies the situation is a little different. The mapping relation, Eq. (45), shows that the integral curve (Fig. 4) can only be continued from $P = V = 1$ to (P_C, V_C), where

$$P_C = (c^2)^{\gamma/\gamma+1} \tag{49}$$

The image of the flowfield in the physical plane turns around if the integral curve is continued past this value. Thus the line $P = P_C$ represents a limit line of the flow, and only for a certain range of $a < a_C$ can the solution be continued to $X = 1$. However, all the solutions for $a > 0$ make sense as flows over nose shapes up to the limit line with a slightly different normalization. Some details of behavior of the integral curve are worked out in Section V.

The integral curve $P(V)$ has been computed numerically for various γ and appears in Fig. 5.** The corresponding

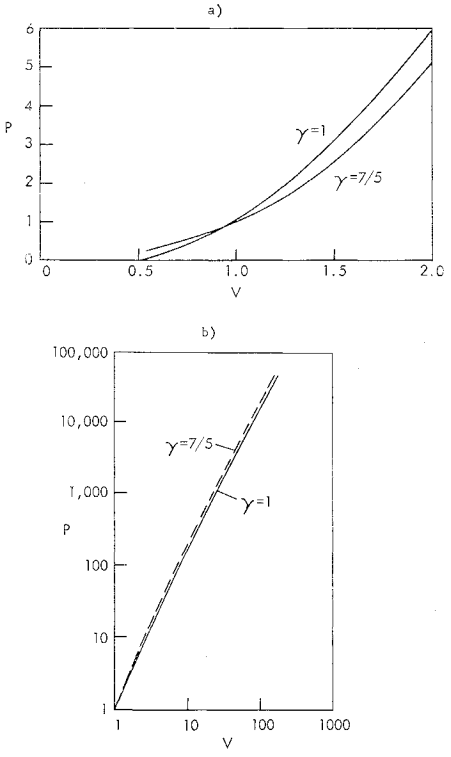

Fig. 5 Integral curves P(V).

** Figure 5 presents results for $\gamma = \frac{7}{5}$. Additional results, for $\gamma = \frac{21}{19}, \frac{11}{9}$, and $\frac{5}{3}$, are included in Ref. 6.

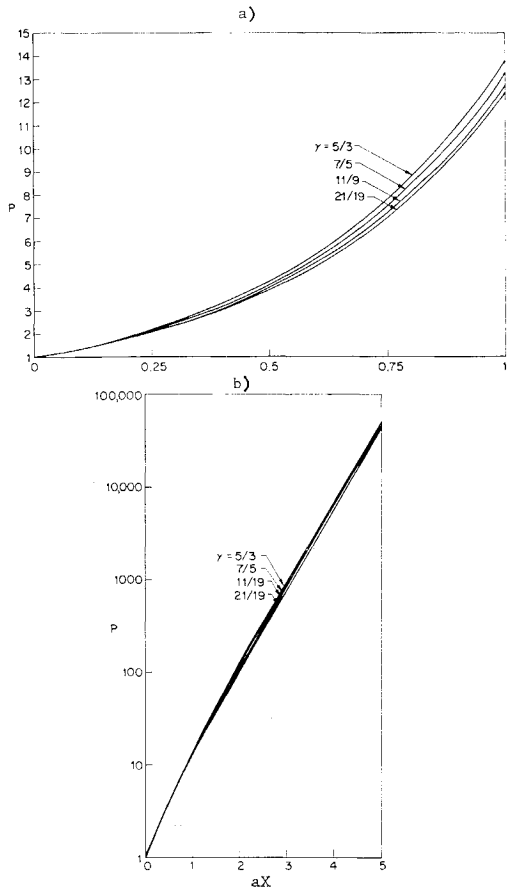

Fig. 6 Universal mapping relation, aX [Eq. (50)].

universal mapping relation

$$aX = \int_1^P \left(1 - \frac{c^2}{P^{(1/\gamma)+1}} \right) \frac{dP}{V(P) + 2P} \tag{50}$$

has been evaluated along this integral curve and the results are presented in Fig. 6. The various pressure distributions and airfoil shapes can be worked out from these curves.

Newtonian Limit

The Newtonian limit[1,4] accounting for impact pressure and centrifugal force corrections appears formally in gas dynamics as the limit $\gamma \to 1$, and correspondingly $\sigma_S \to \infty$. The limit can be applied directly in this example, and it is useful to have these results. Let P_N denote the Newtonian pressure and let $\gamma \to 1$ in Eq. (44). Then

$$dP_N/dV = 1 + 2P_N/V \tag{51}$$

The integral curve passing through (1,1) is thus

$$P_N = 2V^2 - V \tag{52}$$

Since $dP/dV < dP_N/dV$ it is clear that for a given V,

$$P < P_N \text{ for } P > 1,\ a > 0 \text{ (concave case)}$$

$$P > P_N \text{ for } P < 1,\ a < 0 \text{ (convex case)}$$

For this case the mapping relation Eq. (45) becomes simply

$$adX = dV/V \tag{53}$$

or

$$V(X) = e^{aX} = (1/A)F'(X) \tag{54}$$

Thus, in the Newtonian limit, both shock shape and body shape are exponential. It is easy to verify that the usual Newtonian pressure formula for the pressure distribution on

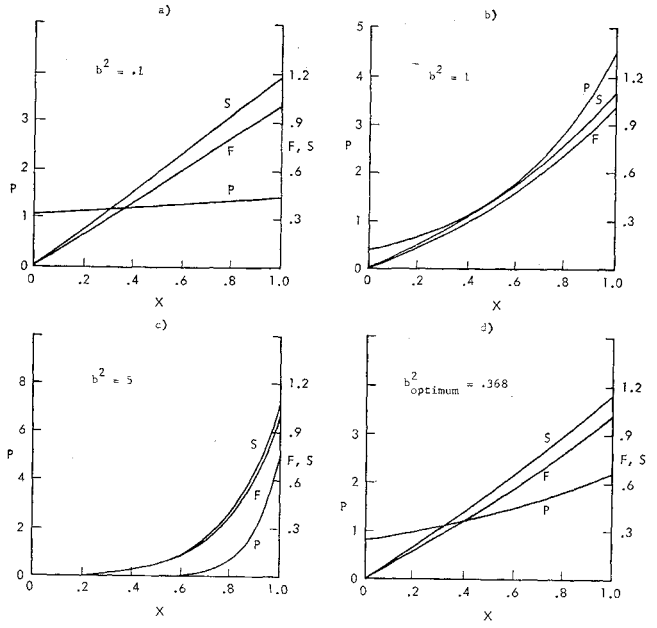

Fig. 7 Concave surfaces supporting exponential shock waves; shock ordinate S, surface ordinate F, pressure P, $\gamma = 7/5$.

a slender body is obtained in this case (see, for example, Ref. 4)

$$P_N(x) = F'^2(x) + F(x)F''(x) = 2A^2e^{2aX} - A^2e^{aX} \quad (55)$$

It is interesting to note that the critical point (P_c,V_c) corresponding to the limit line for the convex nose shapes as $\gamma \to 1$ becomes the point where $P_N \to 0$. This follows from Eq. (49) with $c \to 0$. In Newtonian theory it is assumed that the flow continues past the zero pressure point in the form of a free layer $[S(x) \sim (x)^{1/2}]$. Correspondingly, if $\gamma > 1$ the continuation of the flow past the location of the limit line demands a change in the shock form and body shape. Some details of the problems for concave and convex shapes are discussed in Secs. IV and V.

IV. Concave Shapes; Lift and Drag

For the concave shapes let

$$a = b^2$$

so that the pressure distribution and body slope are represented by

$$p(x,0) = p_b(x) = [2/(\gamma + 1)]A^2P(x) \quad (56)$$

$$v(x,0) = v_b(x) = [2/(\gamma + 1)]AV(x) \quad (57)$$

The shock shape is

$$S(x) = (A/b^2)(e^{b^2x} - 1) \quad (58)$$

From the normalization of Eqs. (48) we have

$$\frac{A}{b^2} = \frac{\gamma + 1}{2} \frac{1}{\{V_T + [(\gamma - 1)/2]P_T^{-(1/\gamma)} - (\gamma + 1)/2\}} \quad (59)$$

Using these results, the pressure distributions, body shapes, and shock shapes for a family of airfoils have been calculated from the universal curves (Figs. 5 and 6). The results are plotted in Fig. 7.

If these concave shapes are regarded as the lower surface of a family of lifting airfoils, explicit formulas for the lift and drag coefficients can be obtained by using the differential equations, Eqs. (40) and (41). Thus Eqs. (56) and (57) show that

$$L = \rho_\infty U^2\delta^2A^2 \frac{2}{\gamma + 1} \int_0^1 P(x)dx \quad (60)$$

$$D = \rho_\infty U^2\delta^3A^3 \left(\frac{2}{\gamma + 1}\right)^2 \int_0^1 P(x)V(x)\,dx \quad (61)$$

The integral in Eq. (60) follows from the momentum equation, Eq. (41)

$$\int_0^1 P(x)\,dx = \frac{1}{2b^2} \int_0^1 \left(\frac{dP}{dx} - \frac{dV}{dx}\right) dx = \frac{1}{2b^2}(P_T - V_T) \quad (62)$$

Again, using Eq. (41),

$$\int_0^1 P(x)V(x)dx = \frac{1}{2b^2} \int_0^1 \left(V\frac{dP}{dx} - V\frac{dV}{dx}\right) dx = \frac{1}{2b^2}\left\{V_TP_T - 1 - \frac{V_T^2}{2} + \frac{1}{2}\right\} - \frac{1}{2b^2}\int_0^1 P\frac{dV}{dx}\,dx$$

Now, using Eq. (40) for dV/dx,

$$\int_0^1 P(x)V(x)dx = \frac{1}{2b^2}\left\{V_TP_T - \frac{V_T^2}{2} - \frac{1}{2}\right\} - \frac{1}{2b^2}\int_0^1 P\left\{\frac{c^2}{P^{(1/\gamma)+1}}\frac{dP}{dx} + b^2V\right\} dx$$

and we see that

$$\frac{3}{2}\int_0^1 P(x)V(x)dx = \frac{1}{2b^2}\left\{V_TP_T - \frac{V_T^2 + 1}{2} - \frac{1}{2}(P_T^{(\gamma-1)/\gamma} - 1)\right\} \quad (63)$$

Thus

$$C_L = \frac{L}{\rho_\infty U^2/2},\ C_D = \frac{D}{\rho_\infty U^2/2}$$

are expressed in terms of the values (V_T,P_T);

$$C_L = \frac{2}{\gamma + 1}\delta^2\frac{A^2}{b^2}\{P_T - V_T\} \quad (64)$$

$$C_D = \frac{2}{3}\left(\frac{2}{\gamma + 1}\right)^2\delta^3\frac{A^3}{b^2}\left\{V_TP_T - \frac{V_T^2}{2} - \frac{1}{2}P_T^{(\gamma-1/\gamma)}\right\} \quad (65)$$

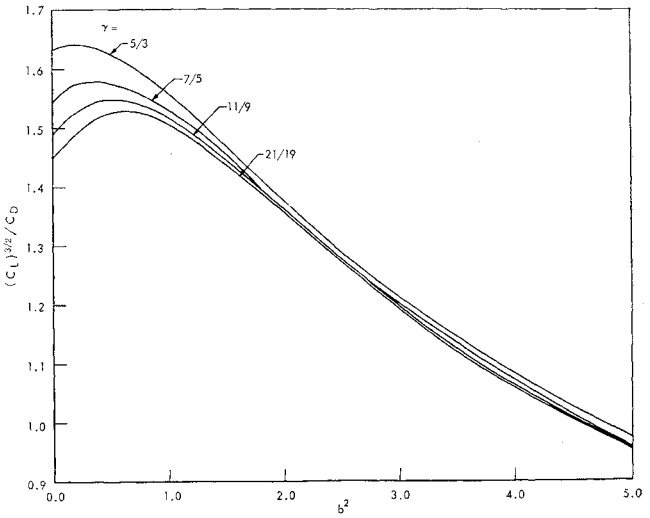

Fig. 8 $(C_L)3/2/C_D$ as a function of nose curvature, b^2 [see Eq. (66)].

The problem of determining the shape producing least drag for a given lift can be studied in terms of the parameter b, representing roughly the curvature of the airfoil, by maximizing $C_L^{3/2}/C_D$

$$\frac{C_L^{3/2}}{C_D} = \frac{3}{2}\left(\frac{\gamma+1}{2}\right)^{1/2}\frac{1}{b}\frac{(P_T - V_T)^{3/2}}{\{V_T P_T - (V_T^2/2) - \frac{1}{2}P_T^{(\gamma-1)/\gamma}\}} \tag{66}$$

The right-hand side of Eq. (66), for a given γ, depends only on the parameter b. Thus a simple maximum for Eq. (66) can be sought. A plot of the curves representing Eq. (66) for various γ is shown in Fig. 8, and C_L/δ^2 is plotted in Fig. 9. The existence of the optimum airfoil within the class of airfoils is easily seen. The shape of the airfoil surface is given in Fig. 7d. The optimum value of $C_L^{3/2}/C_D$ is

$$C_L^{3/2}/C_D = 1.58 \text{ for } \gamma = 1.4 \text{ and } b_{\text{opt}}^2 = 0.368 \tag{67}$$

compared to $(\gamma+1)^{1/2} \approx 1.55$ for a flat surface ($b = 0$).

The limiting Newtonian case can also be studied for comparison with other shapes. As $\gamma \to 1$, Eq. (66) becomes

$$\frac{C_L^{3/2}}{C_D} = \frac{3}{2}\frac{1}{b}\frac{(P_T - V_T)^{3/2}}{V_T P_T - (V_T^2/2) - \frac{1}{2}}$$

or, using Eq. (52),

$$\frac{C_L^{3/2}}{C_D} = \frac{3\cdot 2^{3/2}}{b}\frac{V_T^{3/2}(V_T-1)^{3/2}}{4V_T^3 - 3V_T^2 - 1}$$

or

$$\frac{C_L^{3/2}}{C_D} = \frac{3\cdot 2^{3/2}}{b}\frac{V_T^{3/2}(V_T-1)^{1/2}}{4V_T^2 + V_T + 1} \tag{68}$$

In this case, we have explicitly from Eq. (54),

$$V_T = e^{b^2} \tag{69}$$

The numerical result for the optimum is

$$C_L^{3/2}/C_D = 1.52,\ b = 0.81,\ \gamma = 1 \tag{70}$$

compared to 1.41 for $b = 0$. This can be compared with the optimum within the class of n-power noses in Newtonian theory††:

$$F(x) = x^n,\ C_L^{3/2}/C_D = 1.47,\ n = 1.23\ldots \tag{71}$$

The absolute optimum according to variational calculus and Newtonian theory is worked out by Hayes and Probstein.‡‡ The airfoil is a flat plate from $x = 0$ to $x = 1$ fitted with a chine strip at the tail that increases the flow deflection suddenly by a factor $(3)^{1/2}$

$$(C_L^{3/2}/C_D)_{\text{opt}} = 1.61 \text{ (chine strip)} \tag{72}$$

For a flat plate, Newtonian theory gives

$$C_L^{3/2}/C_D = (2)^{1/2} \tag{73}$$

Thus the optimum airfoil in the class of exponential shapes is superior both to the power law optimum and the flat plate, but is still inferior in effectiveness to the chine strip. These comparisons are only valid for $\gamma \to 1$. Within the context of hypersonic small-disturbance theory for $\gamma \neq 1$, and $M\delta \to \infty$, the calculation of the absolute optimum has not yet been performed. For a lifting surface that is only slightly different from a flat plate,[5] it has been shown that a counterpart of the Newtonian chine strip, if $\gamma \neq 1$, is a flap that is hinged at the k_∞th fraction of the chord length, where

$$k_\infty = \frac{1 - [(\gamma-1)/2\gamma]^{1/2}}{1 + [(\gamma-1)/2\gamma]^{1/2}}$$

†† This corrects a statement in the first paragraph of Ref. 5.
‡‡ Ref. 1, p. 108.

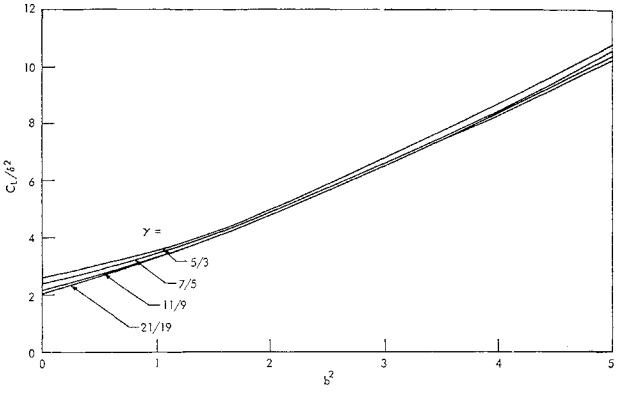

Fig. 9 $C/_L\delta^2$ as a function of noise curvature, b^2.

and is 0.45 for $\gamma = 1.4$. The necessary turning of the shock layer, which can be performed by a chine strip of infinitesimal length if $\gamma = 1$, must be performed by a flap that is almost half the chord length, if $\gamma = 1.4$. Rough qualitative trends for $\gamma \neq 1$ can be inferred from Newtonian theory (i.e., the chine strip-flap correspondence). The results of the present study suggest that for this limited class of airfoils in air ($\gamma = \frac{7}{5}$) the improvement in $C_L^{3/2}/C_D$ over the flat plate value is about 7% if computed by Newtonian theory and only 2% if computed by hypersonic small-disturbance theory. However, although the improvement in performance is greatly overestimated by Newtonian theory, the shapes of the optimum airfoil are not very different.

V. Convex Shapes

For the convex nose shapes let

$$a = -\kappa^2 \tag{74}$$

so that the pressure distribution and body slope are

$$p(x,0) = p_b(X) = [2/(\gamma+1)]A^2P(x) \tag{75}$$

$$v(x,0) = v_b(X) = [2/(\gamma+1)]AV(x) \tag{76}$$

The shock shape is given by

$$S(x) = (A/\kappa^2)(1 - e^{-\kappa^2 x}) \tag{77}$$

The essential feature of the convex nose shapes is the expansion of the flow along the integral curve from $P = 1$ to $P = P_C$ in Fig. 4. We now examine the details of the solution near this critical point

$$P_C = c^{2\gamma/\gamma+1} \tag{78}$$

It can be seen from Eq. (44) that

$$(dP/dV)_C = 1 \tag{79}$$

Thus the integral curve has the local expansion

$$P = P_C + (V - V_C) + \ldots \tag{80}$$

Using this result, the mapping relation Eq. (45) becomes

$$\kappa^2 dX = -\left(1 - \frac{1}{[1 + (V - V_C)/P_C]^{(\gamma+1)/\gamma}}\right) \times \frac{dV}{V_C + 2P_C} + \ldots$$

or

$$\kappa^2 dX = -[(\gamma+1)/\gamma][(V - V_C)/P_C(V_C + 2P_C)]dV \tag{81}$$

The integral curve locally is

$$\kappa^2(X - X_C) = -[(\gamma+1)/2\gamma][1/P_C(V_C + 2P_C)] \times (V - V_C)^2 \tag{82}$$

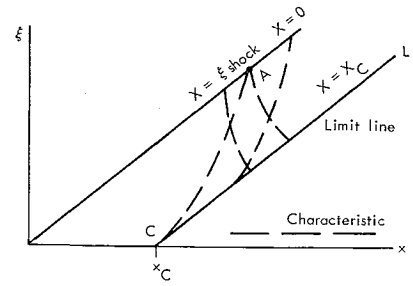

Fig. 10 Convex body detail(x, ξ plane).

Thus

$$V - V_C = \pm\{[2\gamma\varkappa/(\gamma+1)][P_C(V_C + 2P_C)] \times (X_C - X)\}^{1/2} \quad (83)$$

The plus branch of Eq. (83) corresponds to the expanding flow coming up to the critical point. Equation (83) shows that the streamlines in the physical plane must reverse at the critical point, a typical behavior at a limit line. Since $dV/dX \to \infty$ at $X \to X_C$, the curvature of the body (and of all streamlines at X_C) is thus infinite. The line $X = X_C$ has the slope of a characteristic in the physical plane but is not a characteristic. Rather it can be shown that it is the envelope of characteristics (see Fig. 10). This means that the solution with exponential shock shape cannot be continued downstream past this limit line. However, up to the infinite curvature point on the body the solutions make sense.

If $\varkappa^2 \leq \varkappa_{\max}^2$, where $\varkappa_{\max}^2$ is computed from Eq. (50)

$$\varkappa_{\max}^2(\gamma) = \int_{P_C}^{1} \left(1 - \frac{c^2}{p(\gamma+1)/\sigma}\right) \frac{dP}{V(P) + 2P} \quad (84)$$

then $X_C \geq 1$. In the limiting case of $\varkappa^2 = \varkappa_{\max}^2$, the limit line first appears at $X = 1$, the trailing edge of the surface. For these values of $\varkappa^2 \leq \varkappa_{\max}^2$, the standard normalization of Sec. III still applies ($\varkappa_{\max}^2 \approx 0.192$ if $\gamma = \frac{7}{5}$). The airfoil curvature corresponding to $\varkappa_{\max}^2$ is the most convex complete airfoil surface that can support an exponential shock wave. Some of the computed pressure distributions and body shapes are given in Fig. 11.

However, with a different normalization, and a different interpretation to the flowfield, it is possible to imagine a continuation of the flow past the critical point. The exponential shock cannot continue downstream past point A in Fig. 10, which is the first point influenced by the critical point C. By altering the body shape at C so that the curvature is finite, the flow can be continued using conditions on CA as initial data. Thus the exponential shock shape and its supporting airfoil surface from $X = 0$ to $X = X_C$ correspond to only the leading edge of a complete airfoil, extending from $X = 0$ to $X = 1$.

VI. Summary and Conclusions

This study is part of a continuing investigation of airfoil optimization, using the equations of hypersonic gas dynamics. This relatively refined theory must be used since Newtonian theory gives results which are only qualitatively applicable for $\gamma \neq 1$.

The flow behind concave and convex exponential shock waves has been investigated, and the corresponding supporting airfoil surfaces have been determined. The optimum lifting surface which corresponds to an exponential shock wave in terms of maximum $C_L^{3/2}/C_D$ for fixed C_D has been shown to be only slightly more concave than a flat plate, and the improvement in performance over a flat plate is small. A limit line has been shown to exist in the flowfield behind convex exponential shock waves, so that it is not possible to construct an airfoil that supports an exponential shock wave over its entire length if the nose curvature is too large.

It is recognized that applications of lifting hypersonic surfaces may involve prolonged flight at higher altitudes, where viscous effects and forces are significant. For such applications, the results presented here are only a guide to the actual state of affairs, and the inclusion of boundary-layer and three-dimensional effects may be necessary for realistic optimization studies.

Appendix: Similarity Solutions of HSDT Equations

Shock waves which are either exponential or power law permit similarity solutions of the hypersonic small-disturbance (HSDT) equations. This is shown here, using the ξ, x coordinate system.

If $\eta(\xi,x)$ is a similarity variable, and is a constant when $x = \xi$, then the similarity forms

$$p = \theta^2(\xi)P(\eta) \qquad v = \theta(\xi)V(\eta) \quad (A1)$$

are consistent with the boundary conditions at the shock wave.

Replacing these forms in Eqs. (30) and (31) leads to

$$\frac{C^2 P_\eta(\partial\eta/\partial x)}{P^{1/\gamma+1}}\theta + \frac{d\theta}{d\xi}(\xi)V(\eta) + \theta V_\eta \frac{\partial\eta}{\partial\xi} = 0 \quad (A2)$$

$$2\theta\theta' P(\eta) + \theta^2 P_\eta(\partial\eta/\partial\xi) + \theta^2 V_\eta(\partial\eta/\partial x) = 0 \quad (A3)$$

The necessary conditions on θ and η are of the form

$$[(d\theta/d\xi)1/\theta][1/(\partial\eta/\partial x)] = F_1(\eta) \quad (A4a)$$

$$(\partial\eta/\partial\xi)/(\partial\eta/\partial x) = F_2(\eta) \quad (A4b)$$

From Eq. (A4a)

$$\int_0^\eta F_1(\eta')d\eta' = \frac{d\theta}{d\xi}\frac{1}{\theta}x + \phi(\xi) \quad (A5)$$

If η is a constant, η_0, when $x = \xi$, then

$$\int_0^{\eta_0} F_1(\eta')d\eta' = \frac{d\theta}{d\xi}\frac{1}{\theta}\xi + \phi(\xi)$$

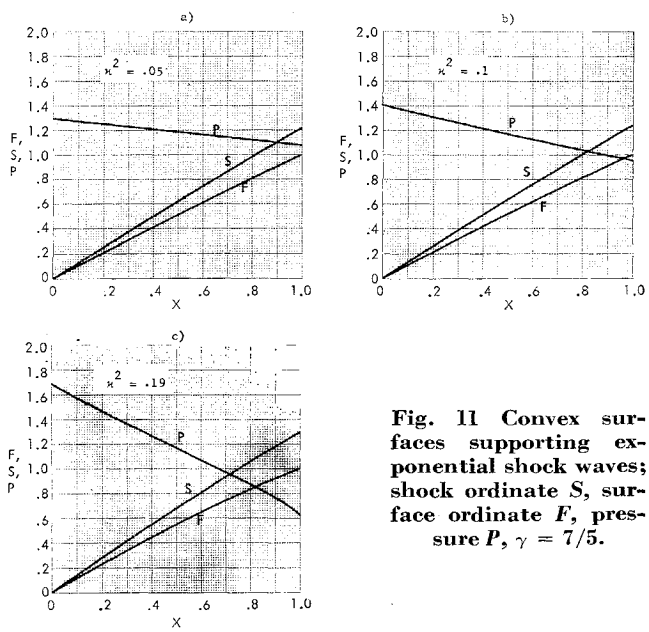

Fig. 11 Convex surfaces supporting exponential shock waves; shock ordinate S, surface ordinate F, pressure P, $\gamma = 7/5$.

or

$$G(\eta) = (d\theta/d\xi)(1/\theta)(x - \xi) \tag{A6}$$

where

$$G(\eta) = \int_{\eta_0}^{\eta} F_1(\eta')d\eta'$$

From Eq. (A6), we obtain

$$\partial G/\partial x = (dG/d\eta)\partial\eta/\partial x = (d\theta/d\xi)1/\theta \tag{A7a}$$

and

$$\frac{\partial G}{\partial \xi} = \frac{dG}{d\eta}\frac{\partial \eta}{d\xi} = (x - \xi)\left(\frac{d^2\theta}{d\xi^2}\cdot\frac{1}{\theta} - \frac{(d\theta/d\xi)^2}{(\theta)^2}\right) - \frac{d\theta}{d\xi}\frac{1}{\theta} \tag{A7b}$$

After these expressions are inserted in Eq. (A4b), and assuming that $dG/d\eta \neq 0$, we arrive at

$$\left[(x - \xi)\left(\frac{d^2\theta}{d\xi^2}\frac{1}{\theta} - \frac{(d\theta/d\xi)^2}{\theta^2}\right) - \frac{d\theta}{d\xi}\cdot\frac{1}{\theta}\right] = F_2(\eta)\frac{d\theta}{d\xi}\frac{1}{\theta} \tag{A8}$$

Using Eq. (A6), this can be written as

$$\left[G(\eta)\frac{\theta_{\xi\xi}}{\theta_\xi}\frac{\theta}{\theta_\xi}\right] = F_2(\eta) + 1 + G(\eta) \tag{A9a}$$

or

$$\frac{\theta_{\xi\xi}}{\theta_\xi}\frac{\theta}{\theta_\xi} = \frac{F_2(\eta) + 1 + G(\eta)}{G(\eta)} \tag{A9b}$$

For this to be true, it is necessary that

$$\frac{\theta_{\xi\xi}}{\theta_\xi}\frac{\theta}{\theta_\xi} = \lambda \tag{A10}$$

where λ is a constant. Then, after integrating,

$$\theta_\xi = a\theta^\lambda \tag{A11}$$

where a is a constant. If $\lambda \neq 1$,

$$\theta = A\{\xi + B\}^{1/1-\lambda} \tag{A12}$$

where A and B are constants. The case $\gamma = 1$ clearly corresponds to the exponential shock wave [from Eq. (A11)], and the case $\gamma \neq 1$ corresponds to the power law shock wave.

References

[1] Hayes, W. D. and Probstein, R. F., "Hypersonic Flow Theory," Vol. 1, *Inviscid Flow*, 2nd ed., Academic Press, New York, 1966, p. 167.

[2] Mirels, H., "Hypersonic Flow Over Slender Bodies Associated With Power-Law Shocks," *Advances in Applied Mechanics*, Vol. VII, edited by H. L. Dryden and T. von Kármán, Vol. VII, Academic Press, New York, 1962, pp. 1–54.

[3] Chernyi, G. G., *Introduction to Hypersonic Flow*, Academic Press, New York, 1961.

[4] Cole, J. D., "Newtonian Flow Theory for Slender Bodies," *Journal of the Aeronautical Sciences*, Vol. 24, 1957, pp. 448–455.

[5] Cole, J. D. and Aroesty, J., "Optimum Hypersonic Lifting Surfaces Closer to Flat Plates," *AIAA Journal*, Vol. 3, No. 8, Aug. 1965, pp. 1520–1522.

[6] Cole, J. D. and Aroesty, J., "Hypersonic Similarity Solutions for Airfoils Supporting Exponential Shock Waves," RM-5724-PR, Aug. 1968, The RAND Corp.

FEBRUARY 1970 AIAA JOURNAL VOL. 8, NO. 2

Cone Drag in Rarefied Hypersonic Flow

M. I. Kussoy* and C. C. Horstman*
NASA Ames Research Center, Moffett Field, Calif.

Experimental drag coefficients for spheres and sharp cones in rarefied hypersonic air flow are presented. These data were obtained using a free-flight technique in a shock tunnel. The test conditions were Mach number from 15 to 24.6, Reynolds number/in. from 690 to 2630, mean free path from 0.009 to 0.053 in., and cone semivertex angles from 2.5° to 25°. When compared with hypersonic viscous interaction and near free molecular theories (both computed for the present range of test conditions), the cone drag is overestimated. However, applying the viscous interaction parameter of Mirels and Ellinwood, a correlation of cone drag for each cone angle in terms of Mach number and freestream Reynolds number is developed. A correlation of average local skin-friction coefficient (deduced from the present data) for individual cone angles is also developed in terms of Mach number and freestream Reynolds number. The ratio of skin-friction to heat-transfer coefficient is shown to be a function only of cone angle.

Nomenclature

C = Chapman-Rubesin viscosity law coefficient ($\mu_w T/\mu T_w$)
C_D = drag coefficient referenced to base area
C_H = Stanton number
$\bar{c}_f$ = average local skin-friction coefficient
Kn = Knudsen number
l = axial length of model
M = Mach number
q = dynamic pressure
Re = Reynolds number
T = temperature
U = velocity
λ = mean free path
θ_c = cone semivertex angle
μ = viscosity

Subscripts

D = diameter
INV = inviscid

Presented as Paper 69-140 at the AIAA 7th Aerospace Sciences Meeting, New York, January 20–22, 1969; submitted February 3, 1969; revision received May 23, 1969.

* Research Scientist. Member AIAA.